

Article

Sulfuric Acid Treated g-CN as a Precursor to Generate High-Efficient g-CN for Hydrogen Evolution from Water under Visible Light Irradiation

Hui-Ju Kang ^{1,†}, Tae-Gyu Lee ^{1,†}, Gazi A. K. M. Rafiqul Bari ¹, Hye-Won Seo ², Jae-Woo Park ¹, Hyun Jin Hwang ², Byeong-Hyeon An ², Norihiro Suzuki ³, Akira Fujishima ³, Jong-Ho Kim ², Ho Kyong Shon ^{4,*} and Young-Si Jun ^{1,2,*}

¹ Department of Advanced Chemicals & Engineering, Chonnam National University, 77 Yongbong-ro, Buk-gu, Gwangju 61186, Korea; gmlwn120@gmail.com (H.-J.K.); dlxorb007@gmail.com (T.-G.L.); grafiquibari@gmail.com (G.A.K.M.R.B.); jaewoopark0218@gmail.com (J.-W.P.)

² School of Chemical Engineering, Chonnam National University, 77 Yongbong-ro, Buk-gu, Gwangju 61186, Korea; hyewonso974@gmail.com (H.-W.S.); wgguswls@gmail.com (H.J.H.); byeonhyeon2021@gmail.com (B.-H.A.); jonghkim@jnu.ac.kr (J.-H.K.)

³ Photocatalysis International Research Center (PIRC), Research Institute for Science and Technology (RIST), Tokyo University of Science, 2641 Yamazaki, Noda, Chiba 278-8510, Japan; suzuki.norihiro@rs.tus.ac.jp (N.S.); fujishima_akira@rs.tus.ac.jp (A.F.)

⁴ Faculty of Engineering and IT, University of Technology, Sydney, P.O. Box 123, Broadway, NSW 2007, Australia

* Correspondence: Hokyong.Shon-1@uts.edu.au (H.K.S.); ysjun@jnu.ac.kr (Y.-S.J.); Tel.: +61-2-95142629 (H.K.S.); +82-62-530-1812 (Y.-S.J.)

† These authors are equally contributed to the work.



Citation: Kang, H.-J.; Lee, T.-G.; Bari, G.A.K.M.R.; Seo, H.-W.; Park, J.-W.; Hwang, H.J.; An, B.-H.; Suzuki, N.; Fujishima, A.; Kim, J.-H.; et al. Sulfuric Acid Treated g-CN as a Precursor to Generate High-Efficient g-CN for Hydrogen Evolution from Water under Visible Light Irradiation. *Catalysts* **2021**, *11*, 37. <https://doi.org/10.3390/catal11010037>

Received: 14 December 2020

Accepted: 29 December 2020

Published: 31 December 2020

Publisher's Note: MDPI stays neutral with regard to jurisdictional claims in published maps and institutional affiliations.



Copyright: © 2020 by the authors. Licensee MDPI, Basel, Switzerland. This article is an open access article distributed under the terms and conditions of the Creative Commons Attribution (CC BY) license (<https://creativecommons.org/licenses/by/4.0/>).

Abstract: Modifying the physical, chemical structures of graphitic carbon nitride (g-CN) to improve its optoelectronic properties is the most efficient way to meet a high photoactivity for clean and sustainable energy production. Herein, a higher monomeric precursor for synthesizing improved micro-and electronic structure possessing g-CN was prepared by high-concentrated sulfuric acid (SA) treatment of bulk type g-CN (BCN). Several structural analyses show that after the SA treatment of BCN, the polymeric melon-based structure is torn down to cyameluric or cyanuric acid-based material. After re-polycondensation of this material as a precursor, the resulting g-CN has more condensed microstructure, carbon and oxygen contents than BCN, indicating that C, O co-doping by corrosive acid of SA. This g-CN shows a much better visible light absorption and diminished radiative charge recombination by the charge localization effect induced by heteroatoms. As a result, this condensed C, O co-doped g-CN shows the enhanced photocatalytic hydrogen evolution rate of 4.57 $\mu\text{mol/h}$ from water under the visible light (>420 nm) by almost two times higher than that of BCN (2.37 $\mu\text{mol/h}$). This study highlights the enhanced photocatalytic water splitting performance as well as the provision of the higher monomeric precursor for improved g-CN.

Keywords: graphitic carbon nitride; sulfuric acid treatment; oxidation and protonation; C, O co-doping; photocatalytic hydrogen evolution; water splitting

1. Introduction

Carbon (IV) nitride (C_3N_4) is a binary compound consisting of alternating C and N atoms [1]. It is classified into three allotropes (molecular, graphitic, and crystal), among which the graphitic phase ($\text{g-C}_3\text{N}_4$) has been computationally calculated to be the most stable allotrope under ambient conditions and of particular importance due to its unique chemical and electronic properties [2]. As an analogue (and complement) of carbon-based graphite, the ideal $\text{g-C}_3\text{N}_4$ consists of tri-s-triazine (or triazine) molecules connected by trigonal N atoms being further extended into 2D graphene-like layers and stacked in a

graphitic fashion. Strong covalent bonds of π -conjugated C and N atoms reinforced by non-covalent π - π interactions between graphene-like layers endow $g\text{-C}_3\text{N}_4$ with excellent chemical (pH 1~14) and thermal stability (up to 600 °C), probably the highest among organic materials [3]. In addition, the sp^2 -hybridized C and N atoms in tri-*s*-triazine molecules generate a semiconducting property whereby electrons transit from N (2p) atoms to C (2p) atoms upon photoexcitation, leaving holes predominantly on N atoms and distributing electrons over tri-*s*-triazine molecules relevant for photocatalytic activity [4]. Furthermore, $g\text{-C}_3\text{N}_4$ features an optical bandgap of ~2.7 eV with highest occupied molecular orbital (HOMO) and lowest unoccupied molecular orbital (LUMO) levels of +1.4 V and -1.3 V (vs. NHE at pH 7), respectively, both straddling the water reduction (-0.41 V vs. NHE at pH 7) and oxidation (+0.82 V vs. NHE at pH 7) potentials [5].

$g\text{-C}_3\text{N}_4$ can be prepared by simple thermal polycondensation of molecular precursors such as dicyandiamide (DCDA), urea, and melamine at high temperatures of 450~600 °C. However, the high-temperature solid-state reaction inevitably accompanies significant mass loss (>60 wt.%) of precursor molecules or intermediate compounds via sublimation and gas evolution, leading to incomplete polycondensation [6]. The resulting materials with uncondensed surface functional groups (-NH_x, x = 1 or 2) or defects such as cyano groups are referred to as polymeric derivatives of the ideal $g\text{-C}_3\text{N}_4$ or polymeric melon ($g\text{-CN}$) [7]. In 2009, Wang et al. for the first time demonstrated that $g\text{-CN}$ enables the photocatalytic water splitting to generate both hydrogen and oxygen under visible light irradiation and active sites for hydrogen evolution are the surface amine functional groups [8]. Given the visible-light-driven photocatalytic activity as well as the earth abundance of constituent elements and chemical/thermal stability, $g\text{-CN}$ could be a viable alternative to supersede the current state-of-the-art photocatalyst, i.e., TiO₂, in a wide variety of applications including solar fuel production, organic synthesis, and pollutants removal [9–11].

The photocatalytic activity of $g\text{-CN}$ in the raw (or bulk or modified) material form is far from ideal (QE of < 0.1%) due to the low visible light absorption and a high degree of charge recombination [8]. As an organic material based on polymer, various (in-)organic synthetic tools offer versatile methods to modify the chemical composition and microstructure of $g\text{-CN}$ and thereby optimize its electronic band structure, optical property, and photocatalytic activity for target reactions. These often include templating, metal (Cu, Fe, Zn) or non-metal (B, O, P, S) doping, defect engineering, etc. [12–14]. For example, nanostructure derived by hard or soft templating increases the catalytically active sites, improves the light-catalyst interaction, shorten the photoexcited charge transfer pathway, and facilitates the mass transfer of reactants and products. The introduction of heteroatoms or defective sites like cyano groups and nitrogen vacancy create (de-)localized or inter-bandgap states which extend the light absorption up to 650 nm and facilitate charge separation/transfer over or among tri-*s*-triazine molecules. It must be noted that these strategies are often counter-balanced: nanostructure induces quantum confinement effect, increasing optical band; heteroatoms (or defects) interrupt the polycondensation process, increasing the degree of charge recombination. The synergistic and cumulative improvement seems to be a challenging task in improving the photocatalytic activity of $g\text{-CN}$.

It is well-known that the polycondensation mode of $g\text{-CN}$ strongly depends on the precursor [15,16]. In particular, the thermal stability of functional groups (-OH, -NH_x, or -SH) and interaction (hydrogen bonding) between the molecular precursors and/or intermediate compounds (DCDA and melamine, MCA and MTCA) are critical factors [17–19]. Inspired by this, we develop a synthetic method based on a partially polymerized precursor to prepare a $g\text{-CN}$ with a high degree of polycondensation. Such a polymeric precursor is prepared by the dissolution of bulk $g\text{-CN}$ (BCN) into high-concentrated sulfur acid (SA) at the high temperature of ~100 °C, leading to complete exfoliation and partial decomposition of tri-*s*-triazine molecules by oxidation. The resulting polymeric precursor is again heated to 550 °C and converted into $g\text{-CN}$ derivatives referred to as BCN/SA-CN. For the characterization, the microstructure was examined by X-ray diffraction (XRD) and N₂ sorption analysis, and the chemical environment was unveiled with Fourier-transform

infrared (FT-IR) spectroscopy, nuclear magnetic resonance (NMR) spectroscopy, and X-ray photoelectron spectroscopy (XPS). To identify the physicochemical-optoelectronic property relationship, UV/Vis diffuse reflectance spectroscopy (DRS), photoluminescence (PL) emission spectroscopy, flat band potential analysis (Mott–Schottky equation), electrochemical impedance spectroscopy (EIS) were conducted. Finally, for the evaluation of photocatalytic activity, catalyst (1 mg/mL) was irradiated with the visible light (>420 nm) within water containing 10 vol.% of triethanolamine (TEOA) and chloroplatinic acid (H_2PtCl_6).

2. Results and Discussion

2.1. Sulfuric Acid Treatment of Bulk Type Graphitic Carbon Nitride (BCN/SA)

Protonation, exfoliation, and dissolution of BCN can be achieved by highly oxidative, high-concentrated sulfuric acid (SA) [20]. BCN (500 mg) is dissolved into SA (1 mL) at 100°C . The slurry solution initially becomes a gel at room temperature due to the chemical bonding between g-CN mesogenic units and is subsequently turned into a clear solution at 100°C (Figure 1a). After SA treatment for 2 h at 100°C , BCN/SA particles are recovered by adding methanol (MeOH) into the BCN/SA solution.

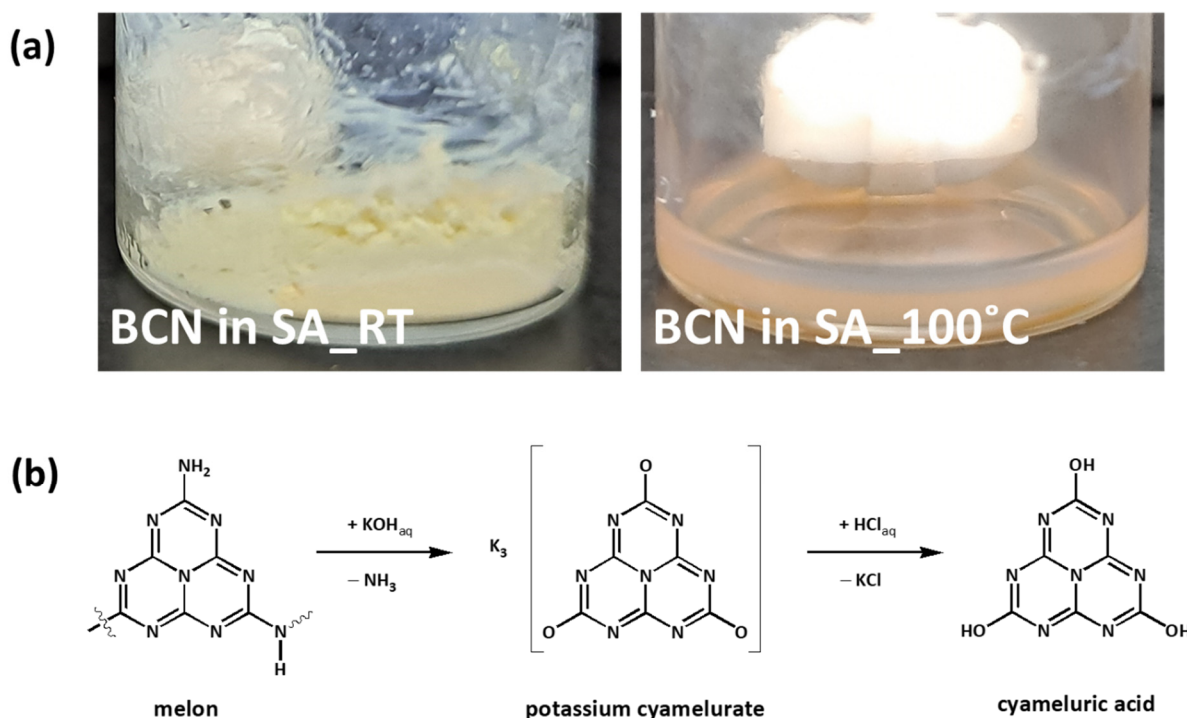


Figure 1. (a) Photo image of bulk g-CN (BCN) dissolved in high-concentrated sulfuric acid (SA) at room temperature (RT) and 100°C , (b) schematic description of the synthesis of cyameluric acid from melon with KOH and HCl treatment [21].

Dissolution of BCN in SA at 100°C induces both protonation and oxidation, which renders it harsher to BCN than individual protonation with aqueous HCl solution or oxidation with aqueous KOH solution under reflux. Similarly to the scheme in Figure 1b, SA converts $-\text{NH}_x$ into $-\text{OH}$ sites in melon or tri-s-triazine unit at high temperatures: a new band corresponding to $-\text{OH}$ stretching mode is emerged at $3000\text{--}3500\text{ cm}^{-1}$, while C–NH–C IR bending mode at $1310\text{--}1230\text{ cm}^{-1}$ is disappeared in FT-IR spectrum of BCN/SA (Figure 2a). The same trend can also be found in both elemental analysis (EA) and XPS: the atomic percentage of oxygen atom increase both from 13.88% to 17.87% and from 3.1% to 22.1%, while that of nitrogen atom decreases both from 47.18% to 35.31% and from 51.6% to 36.9%, respectively (Table 1). Oxidation and subsequent protonation yield monomeric cyameluric (or cyanuric) acid derivatives, shifting the stretching vibration mode of triazine ring from 810 cm^{-1} to 788 cm^{-1} in FT-IR spectra, losing light absorption ability in the

region between 300 and 500 nm in solution UV/Vis absorption spectra and emerging a new peak at 150.3 ppm in liquid-state ^{13}C NMR spectrum attributed to the corner carbon of cyameluric (or cyanuric) acid (Figure 2b–d). An additional peak is accompanied at 141.5 ppm in liquid-state ^{13}C NMR spectrum of BCN/SA-24 h. We attribute this to the bay carbon of cyameluric acid as it is far by 9~10 ppm from that of the corner carbon [21]. Other peaks above 150.3 ppm are, in general, attributed to carbon in R1CONR2, which proves the presence of diverse oxidation products. These are well matched with high-resolution C 1s and N 1s XPS of BCN and BCN/SA. In those spectra, the N–C=N peak is shifted from 279.9 eV to 288.6 eV with much reduced areal contribution (from 80% to 68%) and also the counter C–N=C peak from 398.3 eV to 398.9 eV, respectively (Figure 2e). This distinct shift can be regarded as evidence that significant changes occur in CN heterocycles such as the transformation of terminal C–NH–C to C–OH–C and/or tri-*s*-triazine ring-opening reactions [22].

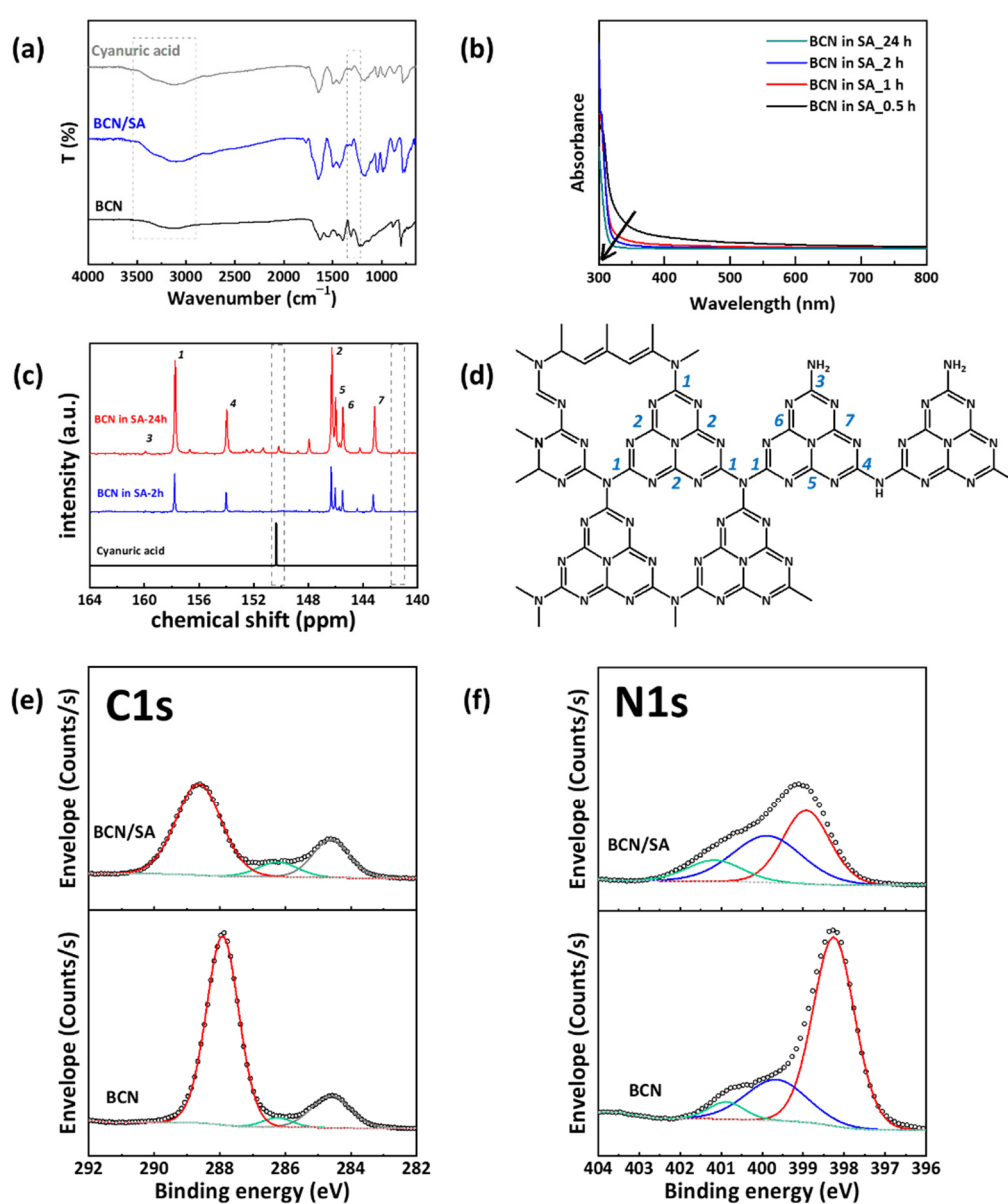


Figure 2. (a) Fourier-transform infrared (FT-IR) spectroscopy of BCN and bulk g-CN/sulfuric acid (BCN/SA) (cyanuric acid (CA) is inserted for the comparison), (b) solution UV/Vis absorption spectroscopy, (c) liquid-state ^{13}C nuclear magnetic resonance (NMR) spectroscopy of BCN dissolved in SA with the increasing time, and (d) schematic description of graphitic carbon nitride structure for assignment of carbon species, high-resolution (e) C 1s, (f) N 1s X-ray photoelectron spectroscopy (XPS) of BCN and BCN/SA.

Table 1. The elemental atomic percentage in BCN and BCN/SA from elemental analysis (EA) (up), XPS survey scan (down).

EA	C (at.%)	N (at.%)	O (at.%)	S (at.%)
BCN	29.51	47.18	13.88	0.01
BCN/SA	24.28	35.31	17.87	3.72
XPS survey	C (at.%)	N (at.%)	O (at.%)	S (at.%)
BCN	45.25	51.59	3.09	0.07
BCN/SA	35.75	36.91	22.12	5.23

The cyameluric (or cyanuric) acid derivatives form rectangular particles in SA as is shown in the polarized optical microscopy (POM) image (Figure 3a). However, monomeric residues are unlikely to survive upon the addition of SA at high temperatures. It was indeed found that mass loss (53%) is severe, and the morphology of g-CN particles are much damaged after dissolution in SA and subsequent precipitation with methanol (Figure 3b). Fiber- or plate-like particles of BCN are absent in SEM images of BCN/SA where aggregates of spherical particles are prevailing. On the other hand, Kroke et al. utilized solution UV/Vis spectroscopy in the pH range between 11.5 and 0.5 in order to observe the step-wise protonation from potassium cyamelurate to cyameluric acid as shown in Figure 1b, glimpsing that tri-*s*-triazine derivatives are stable in the pH range [21]. Moreover, FT-IR and liquid-state ¹³C NMR spectroscopy mentioned above prove the presence of both cyameluric and cyanuric acid derivatives, referred to as higher monomeric residues, in BCN dissolved in SA. We thus assume that the rectangular particles are crystalline material originated essentially from cyameluric or cyanuric acid derivatives in which polymeric melon may coexist before further oxidation (Figure 3a). X-ray diffraction pattern of BCN dissolved in SA shows multiple sharp peaks in the 2θ range between 10° and 30°. These peaks are well matched with those of cyameluric acid with a space group of P2₁2₁2₁, cell lengths (a = 6.4701 Å, b = 9.9340 Å and c = 12.0985 Å), cell angles (α = 90°, β = 90° and γ = 90°) and cell volume of 777.619 Å³, supporting our assumption (Figure 3c,d) [23]. Such ordering is disappeared after mixing with methanol for precipitation, which indicates the instability of the crystal. In addition to the presence of SA, this limits further studies of XRD, TGA, and so on.

The possibility of further decomposition of tri-*s*-triazine into triazine moieties (or lower), i.e., ring-opening reaction, is also evidenced by TGA under a protective gas atmosphere. Proving the presence of cyameluric core N atoms might be a better way, which is, however, highly limited by the fact that protonation of g-CN poses a significant effect on local symmetries by altering graphene-like conformation in solution [20]. Thus, ¹⁵N NMR spectroscopy is unable to distinguish the core N atom. To this end, we rely on thermal analysis like TGA based on thermal stability difference in distinguishing tri-*s*-triazine and triazine derivatives similar to what Cheetham et al. did [24]. The thermal stability of the former is known to be above 500 °C and the latter around 350 °C, which gets slightly lower with the degree of oxidation (or content of oxygen atoms) [8,24]. It is clear from Figure 4a that BCN/SA contains triazine derivatives (or lower), indicating that BCN undergoes ring-opening reaction in the presence of SA at high temperatures. The mass loss resulted from thermal decomposition is accelerated above 300 °C, while BCN without triazine moieties is indeed robust up to 500 °C. It is well known that triazine derivatives are condensed into melon by evolving ammonia at similar temperature ranges [16,25]. This thermal behavior is well reproduced in our system with DCDA, supporting the reliability of the results.

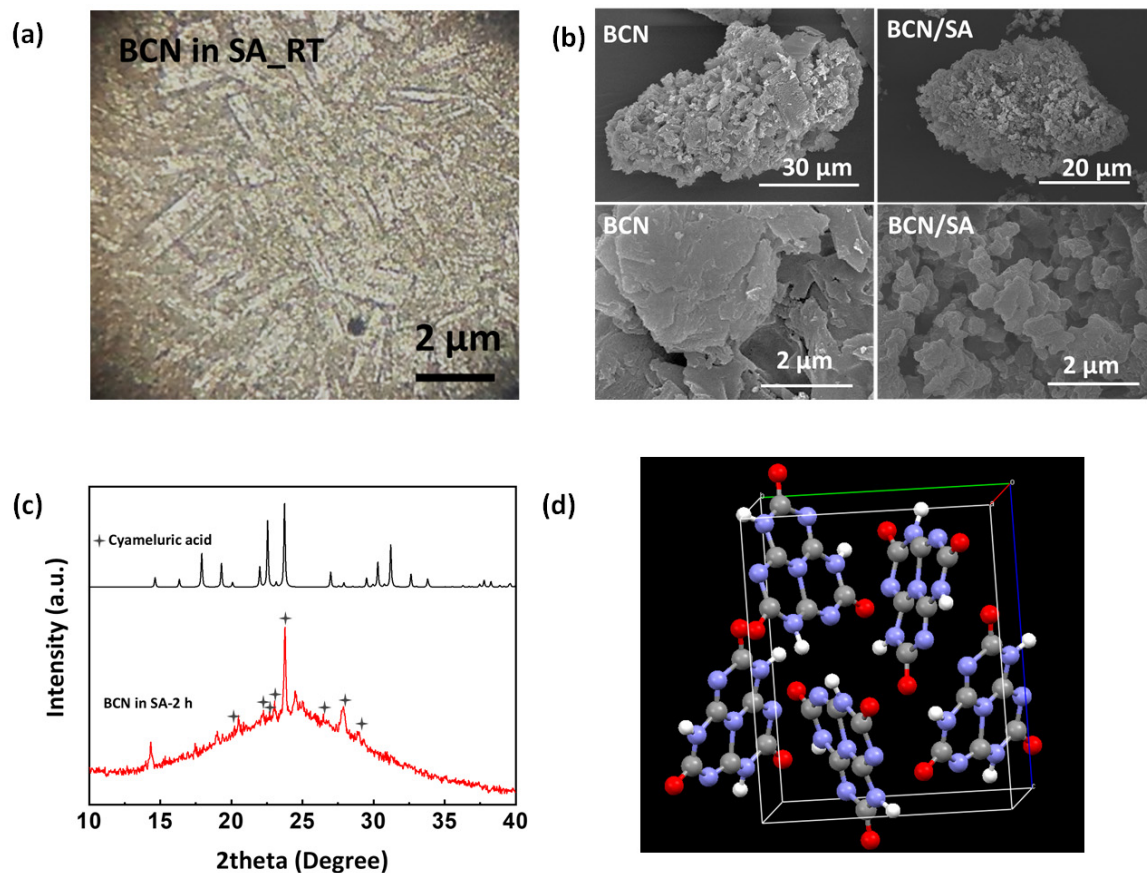


Figure 3. (a) The polarized optical microscopy (POM) image of BCN dissolved in SA for 2 h and then cooled to RT, (b) scanning electron microscopy (SEM) images of BCN and BCN/SA, (c) the X-ray diffraction (XRD) pattern of BCN dissolved in SA for 2 h and then cooled to RT, (d) pattern of cyameluric acid created using cif file with deposition number of 710,788 downloaded from the Cambridge crystallographic data center (CCDC). The crystal structure is created by Mercury 3.0 using the cif file.

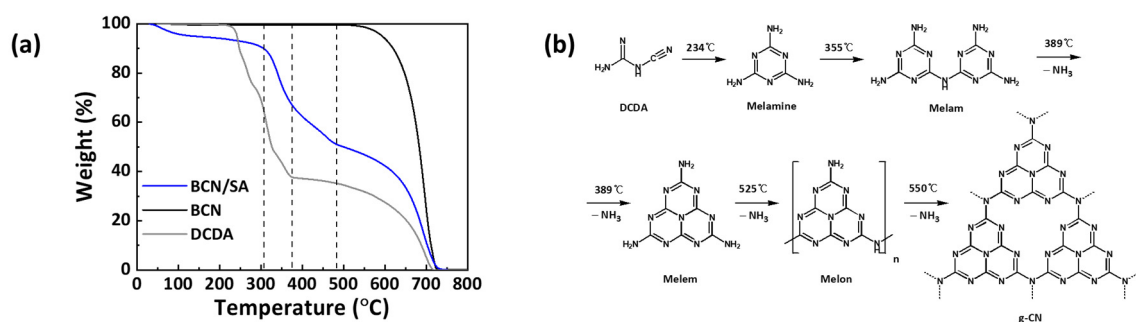


Figure 4. Thermal gravimetric analysis (TGA) of dicyandiamide (DCDA), BCN, BCN/SA (a) and schematic diagram of polymerization of DCDA to g-CN (b) [26].

2.2. Re-Polycondensation of Sulfuric Acid-Treated Graphitic Carbon Nitride Precursor

After re-polycondensation of BCN/SA at 550 °C, the general chemical characteristics of BCN are well recovered in BCN/SA-CN: (1) characteristic CN heterocycles and triazine ring stretching vibration mode of BCN/SA, which is similar to cyanuric acid, turned similarly into those in BCN in the range between 1200 and 1600 cm^{-1} and at 810 cm^{-1} in FT-IR spectra, (2) characteristic two peaks at 157 ppm and 165 ppm appear at the similar position in solid-state ^{13}C cross polarization-magic angle spinning (CP-MAS) NMR spectra

of both BCN and BCN/SA-CN, (3) N=C=N or C=N=C peaks in high-resolution C 1s and N 1s XPS spectra of BCN/SA is shifted back to the lower binding energies similar to those of BCN after re-polycondensation (Figure 5a–c). On the other hand, there is a significant difference between BCN and BCN/SA-CN in terms of atomic contents obtained from EA and XPS analyses: both C, O contents are increased by 0.30%, 0.18% in EA, and 1.60%, 0.96% in XPS, respectively, implying the possibility of C and/or O doping in BCN/SA-CN (Table 2). Such C and O co-doped g-CN was recently achieved with corrosive acids such as H₂SO₄ and HNO₃ by thermal treatment of melamine-acid complex synthesis where C, O co-doping is rather stable than C-doping only [27]. In addition, the powder XRD pattern of BCN/SA-CN shows typical peaks of g-CN at 13.0° and 27.5° corresponding to (100) and (002) reflections resulting from intra-plane and inter-plane ordering of N-bridged tri-s-triazine units (Figure 5d). The lateral size (L_a , 5.71 nm), stacking height (L_c , 2.37 nm), and stacking number (n , 8.25 layers) of graphite-like crystallites embedded in BCA/SA-CN are larger than those of BCN (L_a = 4.73 nm, L_c = 1.50 nm, and stacking number of 5.64), while preserving the interlayer distance (d_{002} = 0.327 nm) between graphene-like layers in BCN/SA-CN close to that of BCN (d_{002} = 0.323 nm). This can obviously be attributed to the sulfuric acid treatment leading to improved degree of polycondensation, which is further corroborated by the decrease in a Brunauer-Emmett-Teller (BET) surface area of BCN/SA-CN (2.1 m²/g) and a pore volume (0.004 cm³/g) compared to those of BCN (3.5 m²/g and 0.020 cm³/g) and BCN/SA (29.6 m²/g and 0.088 cm³/g). (Figure 5e). It should be noted that the degree of polycondensation of g-CN is often counterbalanced by the degree of doping: the higher the doping level, the lower the degree of polycondensation. Such interruption of polycondensation procedures exerted by doping is not observed in BCN/SA-CN, making us to expect the synergistic effects of the high degree of polycondensation and C and O co-doping on reduced charge recombination and improved light absorption, respectively.

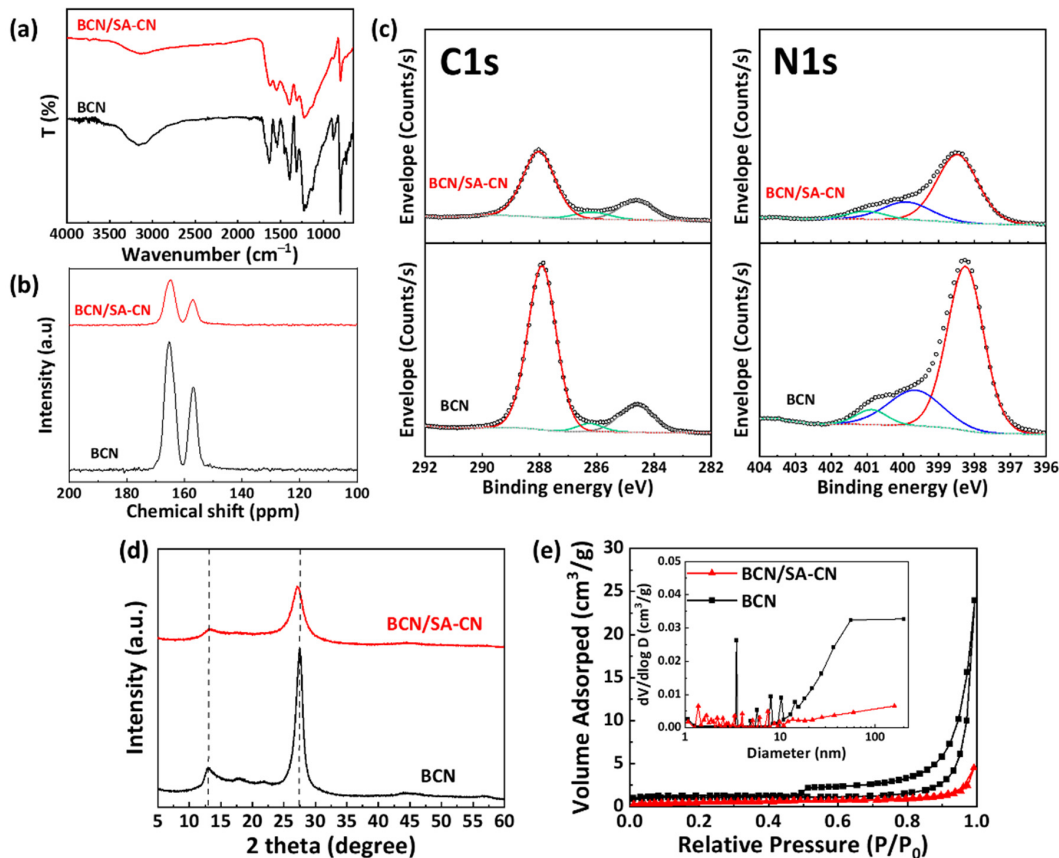


Figure 5. (a) FT-IR spectroscopy, (b) solid-state ¹³C cross polarization-magic angle spinning (CP-MAS) NMR spectroscopy, (c) high-resolution C 1s, N 1s XPS, (d) powder XRD patterns, and (e) N₂ sorption isotherm of BCN and BCN/SA-CN. Inset of (e) is the pore size distribution of BCN and BCN/SA-CN calculated by the Barrett-Joyner-Halenda (BJH) method.

Table 2. Atomic content of each element in BCN and BCN/SA-CN by EA and XPS survey scan.

EA	C (at.%)	N (at.%)	O (at.%)	S (at.%)	C/N Raito
BCN	29.51	47.18	13.88	0.01	0.63
BCN/SA-CN	29.81	44.88	14.06	0.46	0.66
XPS survey	C (at.%)	N (at.%)	O (at.%)	S (at.%)	C/N raito
BCN	45.25	51.59	3.09	0.07	0.88
BCN/SA-CN	46.83	49.02	4.05	0.1	0.96

The effect of the high degree of polycondensation as well as C, O co-doping on optoelectronic properties of BCN/SA-CN was investigated by UV/Vis DRS and PL emission spectroscopy, Mott-Schottky, EIS, photocurrent, and so on. In UV/Vis DRS spectra, BCN/SA-CN shows much enhanced n to π^* transition at the wavelengths over 450 nm region with approximately identical π to π^* transition compared to the pristine BCN due to the much narrower bandgap (2.59 eV vs. 2.84 eV) (Figure 6a–c). In addition to the superior visible light absorption ($\lambda > 450$ nm), BCN/SA-CN shows a much reduced emission spectrum centered on 456 nm, indicating the reduced charge recombination than BCN (Figure 6d). The high degree of polycondensation reduces the population of surface defect sites such as $-\text{NH}_x$ ($x = 1$ or 2) which induces charge recombination. In addition, heteroatoms can localize charges on BCN/SA-CN structure, and thus act as disturbing spots for the recombination of photoexcited electron hole pairs (EHPs) [28]. This is also well shown in electron spin resonance (ESR) spectroscopy in that the localized conjugation system induced by C, O-doping of BCN/SA-CN enable to distribute more lone pair electrons on the LUMO position over the tris-triazine molecules, thus intensify the resonance signal (Figure 6e). Sequentially conducted photocurrent under AM1.5G shows that the BCN/SA-CN exhibits a much larger photocurrent of $2.5 \mu\text{A}/\text{cm}^2$ than that of BCN ($1.5 \mu\text{A}/\text{cm}^2$) (Figure 6f). This is clearly originated from the better absorption of visible light and reduced charge recombination of photogenerated EHPs by charge localization with the presence of heteroatoms, C and O, in BCN/SA-CN structure.

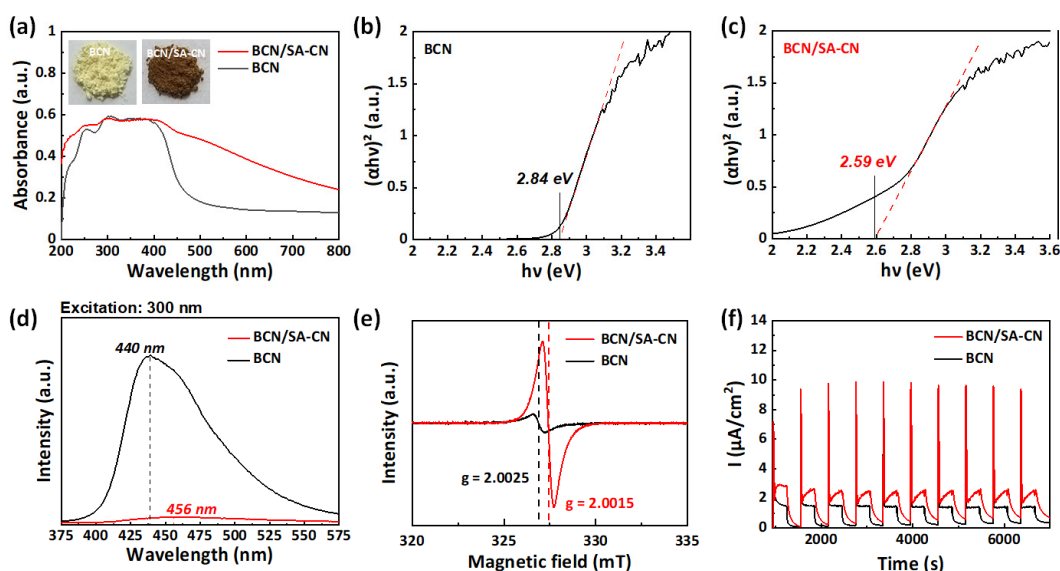


Figure 6. (a) UV/Vis diffuse reflectance spectroscopy (DRS) of BCN and BCN/SA-CN, Tauc-plot of (b) BCN and (c) BCN/SA-CN calculated from UV/Vis DRS by the Kubelka-Munk function, (d) photoluminescence (PL) emission spectroscopy, (e) electron spin resonance (ESR) spectroscopy and (f) photocurrent of BCN and BCN/SA-CN.

Finally, photocatalytic hydrogen evolution reaction (HER) from the water was conducted to evaluate photocatalytic activity of BCN/SA-CN under the visible light (>420 nm)

with the sacrificial electron donor, TEOA. BCN/SA-CN generates an almost two times higher amount of hydrogen during 4 h of photoreaction under the visible light (BCN/SA-CN = 4.57 $\mu\text{mol/h}$, BCN = 2.37 $\mu\text{mol/h}$), which is superior or comparable to those of hetero-atom doped g-CNs (Figure 7a, Table 3). In addition, this catalyst maintains its photocatalytic activity until 16 h of photoreaction (Figure 7b). As shown in Figure 7c, BCN/SA-CN has a more positive HOMO level of -1.44 eV than BCN (-1.81 eV). Interestingly, BCN/SA-CN shows much larger resistance than BCN in electrochemical impedance spectroscopy (EIS), meaning that the charge transfer efficiency of BCN/SA-CN is rather lower than that of BCN (Figure 7d). This is due to the conflict effect of charge localization as explained above, where those heteroatoms also hinder not only the recombination of photogenerated EHPs, but also the efficient charge transfer of them to the surface of photocatalyst. A schematic diagram of overall band structure for each sample was illustrated in Figure 7e. Note that all of the g-CN samples used in this work produce only a negligible amount of hydrogen without TEOA.

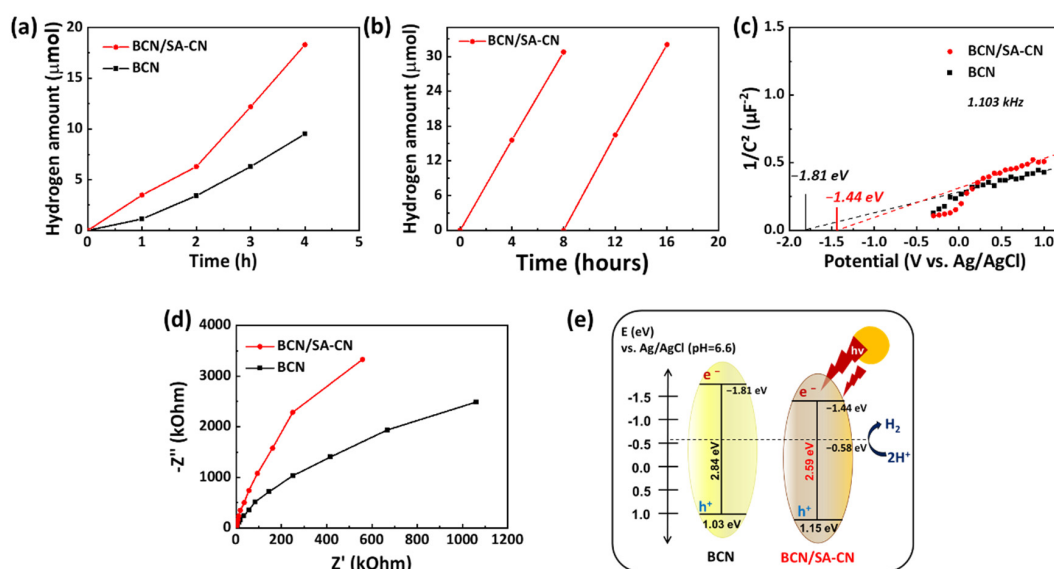


Figure 7. (a) Photocatalytically evolved hydrogen amount with BCN and BCN/SA-CN in 4 h of photoreaction, (b) cycle stability performance of BCN/SA-CN, (c) Mott-Schottky plot of BCN and BCN/SA-CN at frequency 1.103 kHz, (d) electrochemical impedance spectroscopy (EIS) of BCN and BCN/SA-CN at 0.5 V vs. Ag/AgCl (3 M KCl), and (e) schematic description of band structure for BCN and BCN/SA-CN.

Table 3. The performance comparison of photocatalytic hydrogen evolution among g-CN samples.

Material	Cat. (mg)	Donor (vol.%)	Pt (wt.%)	Cat. Conc. (mg/mL)	HER ($\mu\text{mol/h/g}$)	Ref.
BCN	25	TEOA (10)	7	1.00	94.8	This work
BCN/SA	25	TEOA (10)	7	1.00	0	This work
BCM/SA-CN	25	TEOA (10)	7	1.00	182.8	This work
NCN nanosheets	80	TEOA (10)	1	-	115.5	[27]
SCN nanosheets	80	TEOA (10)	1	-	110.5	[27]
g-CN/monoethanolamine	100	MeOH (25)	-	1.25	28.1	[29]
H ₂ SO ₄ /melamine-CN	300	TEOA (10)	0.5	1.50	220	[30]
O-doped g-C ₃ N ₄	100	TEOA (10)	1.2	1.00	375	[31]

3. Materials and Methods

3.1. Materials

The purity and source of purchased reagents are as follows: dicyandiamide (DCDA, 98%, Sigma Aldrich, St. Louis, MO, USA); sulfuric acid (H_2SO_4 , 95~98%, Junsei Chemical Co. Ltd., Tokyo, Japan); dimethyl sulfoxide (DMSO, 99.5%, Daejung, Siheung, Korea); methanol (MeOH, 99.5%, Daejung, Siheung, Korea); sodium hydroxide (NaOH, $\geq 98\%$, Sigma Aldrich, St. Louis, MO, USA); chloroplatinic acid (H_2PtCl_6 , 99.995%, Sigma Aldrich, St. Louis, MO, USA); triethanolamine (TEOA, 99%, Sigma Aldrich, St. Louis, MO, USA). The reagents were used without further purification.

3.2. Synthesis of BCN

An amount of 20 g of dicyandiamide (DCDA) was calcined at 550 °C on the glass container cover a glass lid in the box furnace in the air for 4 h. The heating rate was 2.3 °C/min. After that, yellow-colored bulk-type graphitic carbon nitride was collected and labeled as 'BCN'.

3.3. Synthesis of BCN/SA and BCN/SA-CN

An amount of 500 mg of bulk graphitic carbon nitride (BCN) was added to 1 mL of high concentrated H_2SO_4 (95~98%) and heated to 100 °C for 2 h in an oil bath with a stirring. After that, 40 mL of methanol was added to the solution mixture and jerk well to get a white precipitate. The precipitate was filtered and washed with methanol two times and dried in a vacuum oven at 60 °C overnight. Finally, the white powder was obtained and labeled as 'BNC/SA'. Then, 500 mg of acid-treated bulk g-CN (BCN/SA) was kept on a borosilicate glass vial and heated to 550 °C for 4 h with a ramping rate of 2.3 °C/min. After cooled down, a brownish sample was collected and labeled as 'BCN/SA-CN'.

3.4. Characterizations

To identify the micro-/chemical-structural analysis of materials, the X-ray diffraction (XRD, Rigaku D/max Ultima III instrument with Cu $K\alpha$ radiation ($\lambda = 0.15406 \text{ \AA}$), Rigaku, Tokyo, Japan), elemental analysis (EA, Vario MICRO cube, ELEMENTAR, Langensfeld, Germany, for N, C, H, S and Flash 2000, Thermo fisher, Waltham, MA, USA, for O), X-ray photoelectron spectroscopy (XPS, $K\alpha$ XPS spectrometer, Thermo fisher, Waltham, MA, USA) with a monochromatized micro-focused Al $K\alpha$ line source, and Fourier-transform infrared spectroscopy (FT-IR, JASCO FT-IR 4100 spectrometer, JASCO, Tokyo, Japan), liquid state ^{13}C nuclear magnetic resonance (NMR) spectroscopy (Unity INOVA 500, Varian Co., Palo Alto, CA, USA), solid-state ^{13}C cross polarization-magic angle spinning (CP-MAS) NMR spectroscopy (JNM-EXZ400R, JEOL Ltd., Tokyo, Japan) were conducted. The stacking number is calculated from the L_c value divided by the d_{002} minus 1. Surface morphology was characterized by high-resolution scanning electron microscopy (HR-SEM, Hitachi SU-700, Hitachi, Tokyo, Japan). Nitrogen sorption isotherms were conducted at 77 K (ASAP 2020, Micromeritics, Norcross, GA, USA) to measure the surface area and pore size distribution. Polarized optical microscopy (POM) image was obtained with Eclipse E200 (Nikon Co., Tokyo, Japan). Thermal gravimetric analysis (TGA) was conducted by TGA3 (Mettler Toledo Co., Greifensee, Switzerland). The absorption of ultraviolet and visible light was evaluated by UV/Vis diffuse reflectance spectroscopy (UV/Vis DRS, Lambda 365, Perkin Elmer, Waltham, MA, USA). Materials energy band gap was calculated by using the Kubelka-Munk equation as follows: $F(R) = K/S$; $K = (1-R)^2$; $S = 2R$, where K is molar absorption coefficient, S is scattering factor, and R is reflectance. Liquid state UV/Vis absorption spectroscopy was examined with optizen 3220 UV (NEO Lab. Co., Seoul, Korea). The direct energy bandgap was ascertained by a projection of plotting of $(F(R) hv)^2$ vs. hv . Photoluminescence (PL) emission spectroscopy was carried out using FluoroMax-4 (Horiba, Kyoto, Japan) with an excitation wavelength of 300 nm. Electron spin resonance (ESR) was performed using JES-FA200 (JEOL Ltd., Tokyo, Japan).

3.5. Photoelectrochemical Analysis

A three-electrode cell set up consists of a working electrode, a Pt wire as a counter electrode, and an Ag/AgCl in 3 M KCl as a reference electrode was used to measure the electrochemical properties (photocurrent, electrochemical impedance spectroscopy (EIS), Mott-Schottky analysis) using an electrochemical analyzer (VSP, Seyssinet-Pariset, France, BioLogic). The working electrode was fabricated with FTO (fluorine-doped tin oxide) glass substrate. At first, 50 mg photocatalyst was dispersed in 1.8 mL ethanol and 0.2 mL Nafion solution (5 wt.% in ethanol) by stirring overnight. Then the slurry was drop cast on the substrate and dried in a vacuum oven at 60 °C for overnight (electrode active materials area = 0.5 cm²). The working electrode was engrossed on the supporting electrolyte (0.2 M Na₂SO₄). The cell was purged with nitrogen gas for 30 min to eliminate the air. The perturbation signal is maintained for Mott-Schottky (from −0.3 V to 1.2 V vs. Ag/AgCl, frequency: 100 Hz–200 kHz), EIS (0.5 V vs. Ag/AgCl, frequency: 500 kHz to 4 mHz). Light (100 mW/cm², AM1.5G condition) was irradiated from the rear side of the semiconductor/conductive FTO interface for photocurrent measurement at the steady potential of 0.5 V vs. Ag/AgCl.

3.6. Photocatalytic Activity

In a 50 mL quartz reactor, 25 mg catalyst was dispersed in 25 mL of 3rd DI-water containing 10 vol.% of triethanolamine (TEOA) and 7 wt.% of Pt (H₂PtCl₆, deposition of metallic Pt on the catalyst was done by in-situ photodeposition method). The reaction mixture was kept on stirring for 4 h after that sonication for 1 h and purged with nitrogen for 30 min. The dispersion was irradiated under simulated solar light using 10 suns solar simulator (66902, Newport, Irvine, CA, USA) equipped with 300 W Xenon lamp (6258, Newport, Irvine, CA, USA) as a light source and 420 nm cut-on filter (FSQ-GG420, Newport, Irvine, CA, USA) while keeping the stirring 700 rpm. Finally, a gas chromatogram instrument was used to measure the evolved hydrogen gas (Donam Instruments Inc., Sungnam, Korea, thermal conductive detector, 5 Å molecular sieve column, nitrogen carrier gas).

4. Conclusions

Cyamelic or cyanuric acid-based higher monomeric precursor (BCN/SA) and their derivative g-CN (BCN/SA-CN) was successfully synthesized by high-concentrated sulfuric acid (SA) treatment of BCN and re-polycondensation. Results of structural and optical analyses show that polymeric melon is oxidized and protonated by corrosive acid, H₂SO₄, and the leaved structure is revealed as cyameluric or cyanuric acid-based higher monomeric material. With this material as a precursor, the resulting BCN/SA-CN has a more condensed microstructure and a larger content of carbon and oxygen, indicating the C, O co-doping. These enhance the visible light absorption by reduced bandgap and quenches radiative charge recombination by charge localization effect induced from the presence of heteroatoms in *sp*²-hybridized conjugation system. However, this also intensifies the charge transfer resistance at the same time, where the localization of charge hinders the efficient charge transfer of photogenerated EHPs to the surface of photocatalyst for water splitting reaction. As a result, BCN/SA-CN shows a higher photocatalytic hydrogen evolution rate of 4.57 μmol/h under the visible light irradiation (>420 nm) by almost two times than pristine BCN (2.37 μmol/h).

Author Contributions: Conceptualization, H.-J.K., T.-G.L. and Y.-S.J.; methodology, H.-J.K. and Y.-S.J.; formal analysis, H.-W.S., J.-W.P., H.J.H., B.-H.A.; investigation, H.-J.K., T.-G.L., G.A.K.M.R.B. and Y.-S.J.; data curation, H.-J.K., T.-G.L., H.J.H., J.-W.P.; writing—original draft preparation, H.-J.K.; writing—review and editing, T.-G.L., H.-J.K., G.A.K.M.R.B., H.K.S., J.-H.K., N.S., A.F. and Y.-S.J.; supervision, Y.-S.J.; funding acquisition, J.-H.K. and Y.-S.J. All authors have read and agreed to the published version of the manuscript.

Funding: This research was financially supported by the R&D Convergence Program of NST (National Research Council of Science & Technology) of the Republic of Korea (CAP-15-02-KBSI), the National Research Foundation of Korea (NRF) grant funded by the Korean government (MSIT) (No. 2019R1C1C1007745), Smart Civil Infrastructure Research Program funded by Ministry of Land, Infrastructure and Transport of Korean government, and the National Research Foundation of Korea (NRF) grant funded by the Korean government (Ministry of Science, ICT & Future Planning) (No. 2019R1A4A2001527).

Institutional Review Board Statement: Not applicable.

Informed Consent Statement: Not applicable.

Data Availability Statement: The data presented in this study are available in this article.

Acknowledgments: This study was partly supported by the Joint Usage/Research Program of the Photocatalysis International Research Center, Research Institute for Science and Technology, Tokyo University of Science.

Conflicts of Interest: The authors declare no conflict of interest.

References

1. Kroke, E.; Schwarz, M.; Horath-Bordon, E.; Kroll, P.; Noll, B.; Norman, A.D. Tri-s-triazine derivatives. Part I. From trichloro-tri-s-triazine to graphitic C₃N₄ structures. *New J. Chem.* **2002**, *26*, 508–512. [\[CrossRef\]](#)
2. Saplinova, T.; Bakumov, V.; Gmeiner, T.; Wagler, J.; Schwarz, M.; Kroke, E. 2,5,8-Trihydrazino-s-heptazine: A Precursor for Heptazine-based Iminophosphoranes. *Z. Anorg. Allg. Chem.* **2009**, *635*, 2480–2487. [\[CrossRef\]](#)
3. Thomas, A.; Fischer, A.; Goettmann, F.; Antonietti, M.; Müller, J.-O.; Schlögl, R.; Carlsson, J.M. Graphitic carbon nitride materials: Variation of structure and morphology and their use as metal-free catalysts. *J. Mater. Chem.* **2008**, *18*, 4893–4908. [\[CrossRef\]](#)
4. Lin, T.J.; Chiu, C.C. Influence of nonmetal dopants on charge separation of graphitic carbon nitride by time-dependent density functional theory. *Phys. Chem. Chem. Phys.* **2020**, *22*, 647–657. [\[CrossRef\]](#)
5. Jun, Y.-S.; Lee, E.Z.; Wang, X.; Hong, W.H.; Stucky, G.D.; Thomas, A. From Melamine-Cyanuric Acid Supramolecular Aggregates to Carbon Nitride Hollow Spheres. *Adv. Funct. Mater.* **2013**, *23*, 3661–3667. [\[CrossRef\]](#)
6. Jun, Y.S.; Hong, W.H.; Antonietti, M.; Thomas, A. Mesoporous, 2D Hexagonal Carbon Nitride and Titanium Nitride/Carbon Composites. *Adv. Mater.* **2009**, *21*, 4270–4274. [\[CrossRef\]](#)
7. Lau, V.W.-H.; Moudrakovski, I.; Botari, T.; Weinberger, S.; Mesch, M.B.; Duppel, V.; Senker, J.; Blum, V.; Lotsch, B.V. Rational design of carbon nitride photocatalysts by identification of cyanamide defects as catalytically relevant sites. *Nat. Commun.* **2016**, *7*, 12165. [\[CrossRef\]](#)
8. Wang, X.; Maeda, K.; Thomas, A.; Takanabe, K.; Xin, G.; Carlsson, J.M.; Domen, K.; Antonietti, M. A metal-free polymeric photocatalyst for hydrogen production from water under visible light. *Nat. Mater.* **2009**, *8*, 76–80. [\[CrossRef\]](#)
9. Liao, G.; Gong, Y.; Zhang, L.; Gao, H.; Yang, G.-J.; Fang, B. Semiconductor polymeric graphitic carbon nitride photocatalysts: The “holy grail” for the photocatalytic hydrogen evolution reaction under visible light. *Energy Environ. Sci.* **2019**, *12*, 2080–2147. [\[CrossRef\]](#)
10. Zhang, M.; Bai, X.; Liu, D.; Wang, J.; Zhu, Y. Enhanced catalytic activity of potassium-doped graphitic carbon nitride induced by lower valence position. *Appl. Catal. B Environ.* **2015**, *164*, 77–81. [\[CrossRef\]](#)
11. Zhang, Y.J.; Thomas, A.; Antonietti, M.; Wang, X.C. Activation of Carbon Nitride Solids by Protonation: Morphology Changes, Enhanced Ionic Conductivity, and Photoconduction Experiments. *J. Am. Chem. Soc.* **2009**, *131*, 50–51. [\[CrossRef\]](#) [\[PubMed\]](#)
12. Wang, X.C.; Chen, X.F.; Thomas, A.; Fu, X.Z.; Antonietti, M. Metal-Containing Carbon Nitride Compounds: A New Functional Organic-Metal Hybrid Material. *Adv. Mater.* **2009**, *21*, 1609–1612. [\[CrossRef\]](#)
13. Fu, J.W.; Liu, K.; Jiang, K.X.; Li, H.J.W.; An, P.D.; Li, W.Z.; Zhang, N.; Li, H.M.; Xu, X.W.; Zhou, H.Q.; et al. Graphitic Carbon Nitride with Dopant Induced Charge Localization for Enhanced Photoreduction of CO₂ to CH₄. *Adv. Sci.* **2019**, *6*. [\[CrossRef\]](#) [\[PubMed\]](#)
14. Yu, H.; Shi, R.; Zhao, Y.; Bian, T.; Zhao, Y.; Zhou, C.; Waterhouse, G.I.N.; Wu, L.-Z.; Tung, C.-H.; Zhang, T. Alkali-Assisted Synthesis of Nitrogen Deficient Graphitic Carbon Nitride with Tunable Band Structures for Efficient Visible-Light-Driven Hydrogen Evolution. *Adv. Mater.* **2017**, *29*, 1605148. [\[CrossRef\]](#) [\[PubMed\]](#)
15. Su, Q.; Sun, J.; Wang, J.; Yang, Z.; Cheng, W.; Zhang, S. Urea-derived graphitic carbon nitride as an efficient heterogeneous catalyst for CO₂ conversion into cyclic carbonates. *Catal. Sci. Technol.* **2014**, *4*, 1556–1562. [\[CrossRef\]](#)
16. Bojdys, M.J.; Müller, J.-O.; Antonietti, M.; Thomas, A. Ionothermal Synthesis of Crystalline, Condensed, Graphitic Carbon Nitride. *Chem. Eur. J.* **2008**, *14*, 8177–8182. [\[CrossRef\]](#)
17. Algara-Siller, G.; Severin, N.; Chong, S.Y.; Bjorkman, T.; Palgrave, R.G.; Laybourn, A.; Antonietti, M.; Khimyak, Y.Z.; Krasheninikov, A.V.; Rabe, J.P.; et al. Triazine-Based Graphitic Carbon Nitride: A Two-Dimensional Semiconductor. *Angew. Chem. Int. Edit.* **2014**, *53*, 7450–7455. [\[CrossRef\]](#)
18. Zhang, G.G.; Zhang, J.S.; Zhang, M.W.; Wang, X.C. Polycondensation of thiourea into carbon nitride semiconductors as visible light photocatalysts. *J. Mater. Chem.* **2012**, *22*, 8083–8091. [\[CrossRef\]](#)

19. Jun, Y.-S.; Park, J.; Lee, S.U.; Thomas, A.; Hong, W.H.; Stucky, G.D. Three-Dimensional Macroscopic Assemblies of Low-Dimensional Carbon Nitrides for Enhanced Hydrogen Evolution. *Angew. Chem. Int. Ed.* **2013**, *52*, 11083–11087. [[CrossRef](#)]
20. Zhou, Z.X.; Wang, J.H.; Yu, J.C.; Shen, Y.F.; Li, Y.; Liu, A.R.; Liu, S.Q.; Zhang, Y.J. Dissolution and Liquid Crystals Phase of 2D Polymeric Carbon Nitride. *J. Am. Chem. Soc.* **2015**, *137*, 2179–2182. [[CrossRef](#)]
21. El-Gamel, N.E.A.; Seyfarth, L.; Wagler, J.; Ehrenberg, H.; Schwarz, M.; Senker, J.; Kroke, E. The Tautomeric Forms of Cyameluric Acid Derivatives. *Chem. Eur. J.* **2007**, *13*, 1158–1173. [[CrossRef](#)] [[PubMed](#)]
22. Miller, T.S.; Jorge, A.B.; Suter, T.M.; Sella, A.; Corà, F.; McMillan, P.F. Carbon nitrides: Synthesis and characterization of a new class of functional materials. *Phys. Chem. Chem. Phys.* **2017**, *19*, 15613–15638. [[CrossRef](#)] [[PubMed](#)]
23. Seyfarth, L.; Sehnert, J.; El-Gamel, N.E.A.; Milius, W.; Kroke, E.; Breu, J.; Senker, J. Structure elucidation of cyameluric acid by combining solid-state NMR spectroscopy, molecular modeling and direct-space methods. *J. Mol. Struct.* **2008**, *889*, 217–228. [[CrossRef](#)]
24. Horvath-Bordon, E.; Kroke, E.; Svoboda, I.; Fuess, H.; Riedel, R.; Neeraj, S.; Cheetham, A.K. Alkalicymelurates, M-3 C₆N₇O₃ center dot xH(2)O, M = Li, Na, K, Rb, Cs: UV-luminescent and thermally very stable ionic tri-s-triazine derivatives. *Dalton Trans.* **2004**, 3900–3908. [[CrossRef](#)] [[PubMed](#)]
25. Sattler, A.; Pagano, S.; Zeuner, M.; Zurawski, A.; Gunzelmann, D.; Senker, J.; Muller-Buschbaum, K.; Schnick, W. Melamine-Melem Adduct Phases: Investigating the Thermal Condensation of Melamine. *Chem. Eur. J.* **2009**, *15*, 13161–13170. [[CrossRef](#)] [[PubMed](#)]
26. Groenewolt, M.; Antonietti, M. Synthesis of g-C₃N₄ nanoparticles in mesoporous silica host matrices. *Adv. Mater.* **2005**, *17*, 1789–1792. [[CrossRef](#)]
27. Gao, X.; Feng, J.; Su, D.; Ma, Y.; Wang, G.; Ma, H.; Zhang, J. In-situ exfoliation of porous carbon nitride nanosheets for enhanced hydrogen evolution. *Nano Energy* **2019**, *59*, 598–609. [[CrossRef](#)]
28. Jiang, L.; Yuan, X.; Pan, Y.; Liang, J.; Zeng, G.; Wu, Z.; Wang, H. Doping of graphitic carbon nitride for photocatalysis: A review. *Appl. Catal. B Environ.* **2017**, *217*, 388–406. [[CrossRef](#)]
29. Meng, J.; Lin, Q.; Wu, S.; Pei, J.; Wei, X.; Li, J.; Zhang, Z. Hybrid CN-MEA microplates with enhanced photocatalytic hydrogen evolution under visible light irradiation. *Catal. Sci. Technol.* **2017**, *7*, 3777–3784. [[CrossRef](#)]
30. Yan, H.; Chen, Y.; Xu, S. Synthesis of graphitic carbon nitride by directly heating sulfuric acid treated melamine for enhanced photocatalytic H₂ production from water under visible light. *Int. J. Hydrog. Energy* **2012**, *37*, 125–133. [[CrossRef](#)]
31. Li, J.; Shen, B.; Hong, Z.; Lin, B.; Gao, B.; Chen, Y. A facile approach to synthesize novel oxygen-doped g-C₃N₄ with superior visible-light photoreactivity. *Chem. Commun.* **2012**, *48*, 12017–12019. [[CrossRef](#)] [[PubMed](#)]